

μMap-FFPE: A High-Resolution Protein Proximity Labeling Platform for Formalin-Fixed Paraffin-Embedded Tissue Samples

Noah B. Bissonnette,¹ Marie E. Zamanis,² Steven D. Knutson,¹ Zane Boyer,¹ Angelo Harris,² Daniel Martin,² Jacob B. Geri,¹ Suzana Couto,² Tahamtan Ahmadi,² Anantharaman Muthuswamy,² Mark Fereshteh,² David W. C. MacMillan^{1,*}

1. Merck Center for Catalysis at Princeton University, Princeton, New Jersey 08544, United States

2. Genmab US, Inc., Building 2, 777 Scudders Mill Rd, Princeton, New Jersey 08540, United States

Proximity Labeling, FFPE Tissue, B-cell Lymphoma

ABSTRACT: Many disease states can be understood by elucidating small-scale biomolecular protein interaction networks, or microenvironments. Recently, photoproximity labeling methods, like μMap, have emerged as high-resolution techniques to study key spatial relationships in subcellular architectures. However, *in vitro* models typically lack cell type heterogeneity and three dimensionality, integral parameters that limit the translation of *in vitro* findings to the clinic. To this end, formalin-fixed paraffin-embedded (FFPE) tissues serve as an invaluable model system for biomedical research by fixing complex multi-cell interaction networks in their natural environment. Thus, identifying microscale interactions in these samples would provide important clinical insight. Yet, the underlying chemistry of photoproximity labeling is challenged by formalin-fixation and de-crosslinking, precluding its application. Herein, we report the development of competent labeling system, μMap-FFPE, enabling the comparison of CD20's interactome between healthy and cancerous cells or preserved patient tissues.

Biological interaction networks, comprised of the complex associations of proteins, nucleic acids, and metabolites, orchestrate cellular processes such as signal transduction and gene expression. Additionally, dysregulation of these networks leads to disease phenotypes; thus, understanding signaling pathways is of high clinical relevance for drug development.¹⁻⁴ Yet, elucidating these *in vivo* connections is complicated, as protein-protein interactions can change drastically between a laboratory scale, reductionist model system—often homogenous, immortalized cell lines—and patients in the clinic.⁵⁻⁷ This is driven by *in vivo* features, such as cell type heterogeneity and three dimensionality, being poorly captured by typical cellular models.⁸ The inability to accurately profile these features contributes to the challenge of translating a potent cell-based therapeutic to an approved drug.⁹ New tools are needed to better understand changes in protein interactomes between model types.¹⁰

Photocatalytic proximity labeling is an emerging technology capable of probing microscale interactions.^{11,12} Many labeling platforms have been introduced to date, that enable exploration of these interactions in a variety of biological contexts.¹³ Yet, most methods were developed specifically for simple cellular model systems and may require genetic engineering to install the labeling ensemble,¹⁴⁻¹⁷ precluding their use in tissue samples. Although some methods have been shown to be compatible with complex biological samples like whole blood,¹⁸ there is a dearth of *high-resolution techniques* applicable to human tissue. Recently, Fadeyi and coworkers disclosed a near-infrared proximity labeling

system capable of labeling whole tissue using fluoroalkyl iodides and an organic photocatalyst.¹⁹ Similar advancements demonstrate the tractability of tissue photolabeling with Ir or porphyrin-based catalysts,²⁰⁻²² yet published techniques utilize freshly harvested tissue samples for LC-MS/MS proteomics. This feature significantly limits applications, as the most readily available forms of human tissue are formalin-fixed paraffin-embedded samples (FFPE). Unlike fresh tissue, FFPE samples are stable for decades.²³ Estimates of worldwide FFPE samples range from 400 million to >1 billion (across 1,000s of disease states), overall representing a wealth of clinical information.^{24,25} However, fixation fundamentally alters the molecular identity of the sample, greatly complicating sample preparation and analysis with traditional LC-MS/MS techniques, and its effect on photoproximity labeling mechanisms is poorly understood.²⁶

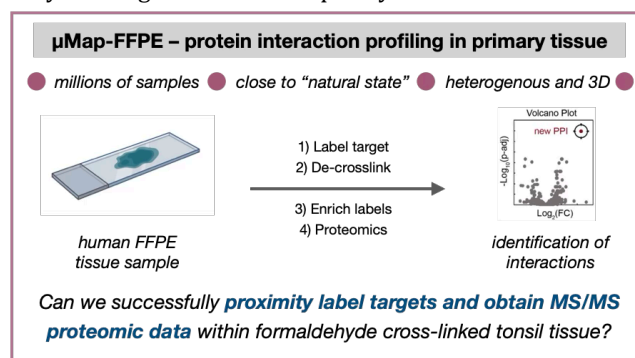


Figure 1: Development of μMap-FFPE.

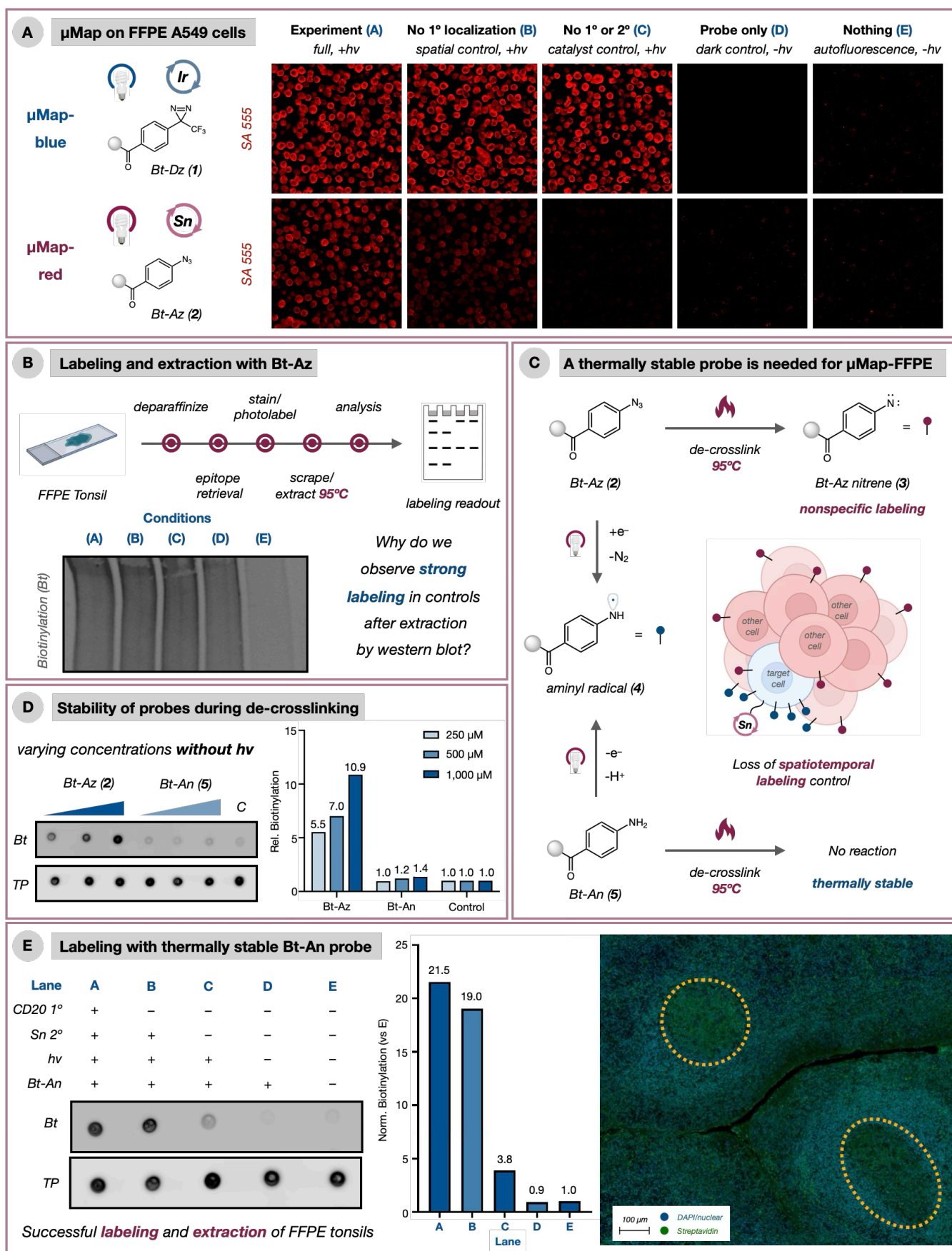


Figure 2: Incompatibility of μMap-blue/red with FFPE samples. (A) Photoproximity labeling of FFPE A549 cells (biotinylation in red). (B) μMap-red with FFPE tonsil. (C) Thermal instability of Bt-Az probe causes nonspecific labeling. (D) Comparison of probe stability during de-crosslinking. (E) Successful CD20 labeling on FFPE tonsil.

Thus, we set out to develop a photoproximity labeling platform capable of generating LC-MS/MS proteomics information with FFPE biological samples (**Figure 1**). Upon developing a labeling manifold for FFPE samples and studying its labeling mechanism, we then examined the interactome of CD20, a B-cell marker and the target of multiple FDA-approved monoclonal antibodies,^{27,28} in human tissue. We also compared the CD20 interaction network across single cell type cultures and tissues, finding fundamental differences in the interactomes of these model systems. Finally, we validated novel CD20 proximal proteins identified by μ Map-FFPE using super-resolution microscopy (STED).²⁹

We first attempted labeling on FFPE cancer cells with our standard μ Map-Blue platform, which uses an Ir catalyst to activate a diazirine probe.¹¹ Surprisingly, irrespective of antibody loading, washing protocol, and epitope retrieval technique, significant background labeling was observed by microscopy. Strikingly, when the Ir catalyst was omitted entirely, we observed nonspecific, blue-light mediated photoactivation upon addition of the diazirine probe (**1**) (**Figure 2a**, conditions C). Diazirenes are not activated by blue-light wavelengths, as they only absorb UV light. This implicates an endogenous photosensitizing capability of the FFPE sample, perhaps arising from the fixation process itself. Indeed, similar results were obtained by western blot using in-house cultured HEK293T cells after formalin-crosslinking (**Figure S1**). This suggests the natural presence or formalin induced formation of a blue-light photosensitizer and rendering μ Map-Blue techniques incompatible with FFPE samples. Interestingly, this formalin-linked mediated background activation was wavelength dependent; it was not observed with our μ Map-Red platform, which uses a Sn-chlorin catalyst to activate an azide probe (**2**) (**Figure 2a**).¹⁸ Using μ Map-Red we sought to identify the interactors of CD20 in FFPE human tonsils with label-free LC-MS/MS proteomics. This requires harvesting the tissue with a razor blade, chemically de-crosslinking and solubilizing the tissue,³⁰ and finally enriching the biotinylated proteins with streptavidin-coated magnetic beads.

Many methods exist for reconstituting FFPE tissue: we sought to identify conditions that maximize recovery of free CD20 and total protein.³¹ We tested several published protocols and buffer solutions and found that 4% SDS, 80 mM HEPES, 80 mM DTT, pH 8 ("buffer B") was optimal (**Figure S2**).³² Furthermore, cells that were formalin-fixed then de-crosslinked using these conditions gave identical band patterns by western blot (**Figure S3**), indicating reconstitution to a "native-like" state, a requirement for successful identification by label-free MS-MS techniques.²⁶ However, when this protocol was applied to μ Map-Red labeled samples, significant biotinylation was observed by western blot for all conditions where Bt-Az (**2**) was added (**Figure 2b**, lanes A-D). Given the contrast to our microscopy studies, we hypothesized that the conditions utilized for decrosslinking (95°C) may promote thermal activation of residual Bt-Az probe, forming a nitrene (**3**).^{33,34} This nitrene nonspecifically label proteins,^{35,36} eliminating spatiotemporal information (**Figure 2c**). Unfortunately, attempts to wash away residual probe before de-crosslinking were unsuccessful.

Recognizing the incompatibility of our photolabeling systems with FFPE samples, we sought to redesign μ Map-Red

to overcome these challenges. Under the standard μ Map-Red platform, **2** is converted to the active aminyl radical (**4**) via reduction by photogenerated Sn(III) followed by N₂ loss and protonation.¹⁸ Cognizant of the key intermediacy of an aminyl radical, we questioned if this species could instead be generated by reductive quenching of the excited Sn^{IV} catalyst (Sn^{IV}/Sn^{III} E_{1/2}^{ox} = 1.25 V) with a biotin aniline conjugate, **5** (Bt-An, E_{p/2} = 0.71 V vs Ag/AgCl). We speculated that a thermally stable aniline probe could avoid nonspecific labeling during heat-induced de-crosslinking (**Figure 2c**). We evaluated the relative thermal stability of Bt-Az (**2**) and Bt-An (**5**) under de-crosslinking conditions, and **5** predictably showed minimal thermal activation whereas **2** participated in significant thermal labeling (**Figure 2d**). Furthermore, when the Sn/aniline system was utilized for proximity labeling of CD20 in FFPE human tonsil slides, labeling (after extraction) was only observed in the presence of the Sn photocatalyst. Thus, a thermally stable, photoproximity labeling system (μ Map-FFPE) was successfully realized. Further optimization of the epitope retrieval conditions improved targeted labeling above background (lane A vs B) to ~2:1. Gratifyingly, a strong biotinylation signal can be observed at germinal centers on FFPE tonsil slides (consistent with the localization of B-cells in tissue, **Figure 2e**).³⁷

With a new probe in hand, we next evaluated the mechanism of activation and subsequent labeling (see SI for extended discussion). Pleasingly, Bt-An labeling conditions were subject to photonic control, implicating the catalytic relevance of excited Sn (**Figure 3a**). However, *in vitro* labeling studies on bovine serum albumin (BSA) and carbonic anhydrase (CA) complicated analysis. Presuming a redox mechanism, a sacrificial oxidant, oxygen, is required to turn over the photocatalyst. Yet, labeling was observed under anaerobic conditions for BSA, though *not* CA. This finding suggests an alternative pathway, wherein interchain disulfide bonds (E_{1/2}^{red} ≥ -0.71 V vs SCE),³⁸ present in BSA but not CA, can serve as oxidants (**Figure 3b**). This hypothesis is supported by the restoration of CA labeling under anaerobic conditions when proteins with disulfide bonds are added (**Figure S4**). These results suggest that a redox labeling mechanism is operative under N₂. However, our analysis for aerobic conditions is complicated by an additional, well-characterized proximity labeling mechanism.^{14,15,39-42} This alternative pathway relies on sensitization of oxygen (**8**) by an excited state catalyst (**7**). Subsequently, ¹O₂ (**9**), can covalently modify nearby residues such as histidine (**10**), *via* [3+2] cycloaddition and ring opening to furnish an electrophile (**11**). These oxidized residues are known to undergo nucleophilic attack with anilines to generate the covalently tagged species (**12**).⁴³ Given the different residue modifications obtained through the two labeling mechanisms (+Bt-An vs +O₂-Bt-An), we sought to implicate the primary pathway by detecting the adduct with DDA LC-MS/MS proteomics using open residue modification search. Interestingly only mass shifts corresponding to the ¹O₂ pathway were identified (+O₂-Bt-An), implicating oxygen sensitization as the dominant labeling pathway (**Figure 3c**). However, we cannot rule out a mixed redox/sensitization mechanism given the successful labeling of BSA under nitrogen. Thus, we propose that under aerobic conditions ¹O₂ is the primary reactive intermediate, while under anaerobic conditions the aminyl radical is responsible for labeling (**Figure 3d**).

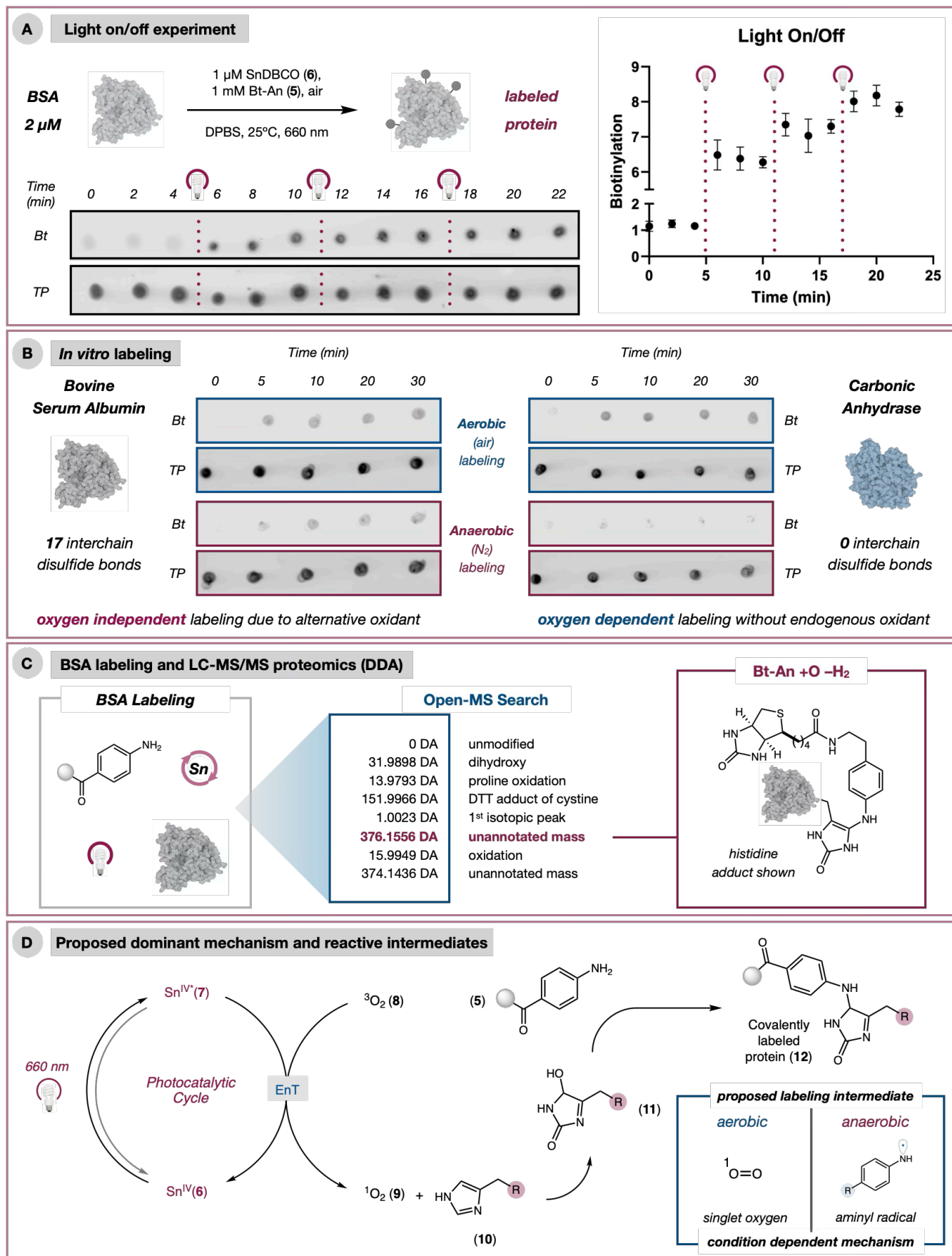


Figure 3: Mechanistic studies for μ Map-FFPE. (A) Light on/off labeling. (B) *In vitro* labeling. (C) Detection of Bt-An-BSA labeling adduct under O₂ by LC-MS/MS DDA. (D) Proposed labeling mechanism and intermediates.

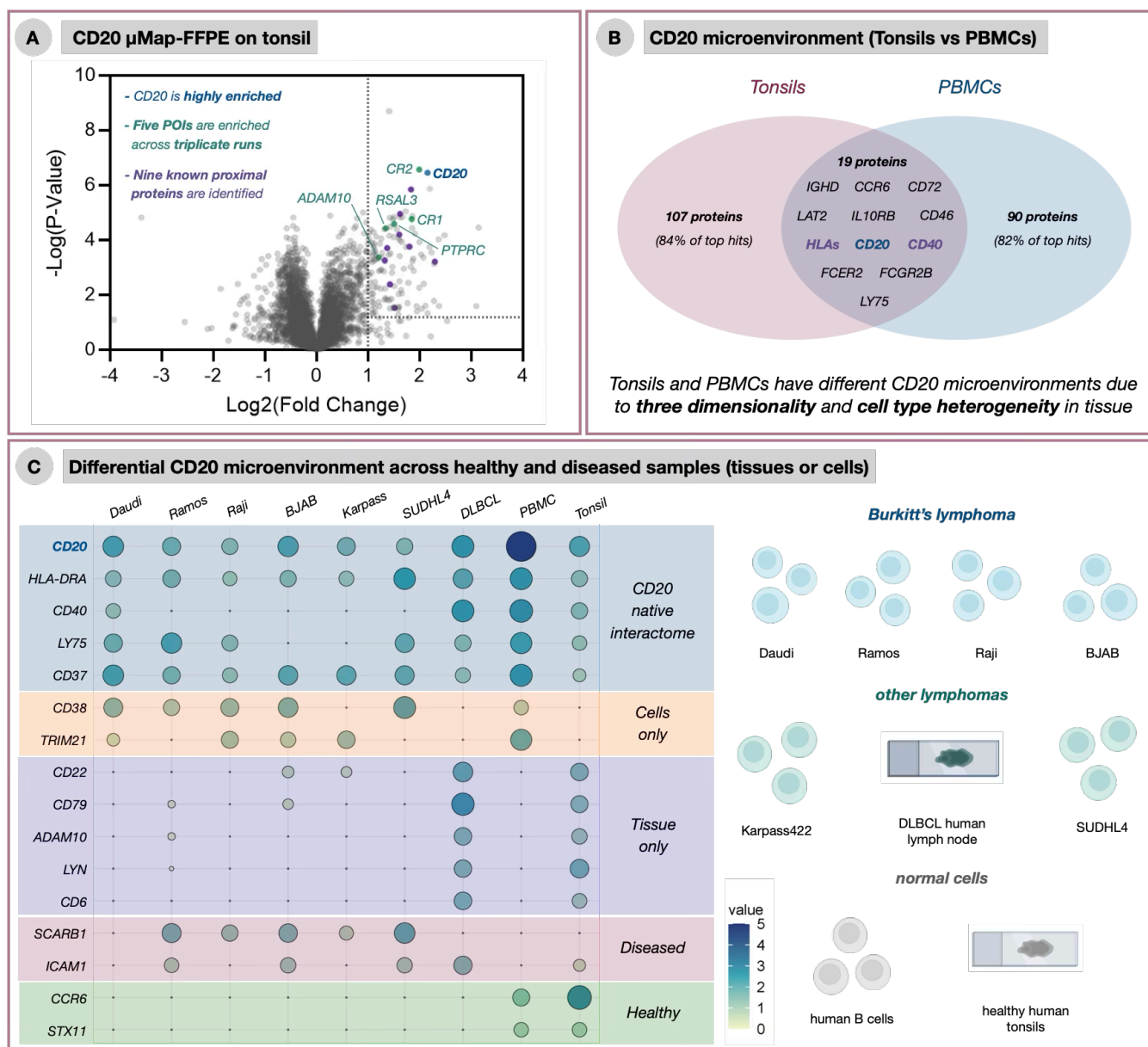


Figure 4: Photoproximity labeling of CD20 on B-cell lines and human tissue. (A) μ Map-FFPE on tonsils. (B) Comparison of CD20 interactome in PBMCs and tonsils. (C) Balloon plot summarizing the CD20 interactome across models.

With a better understanding of the μ Map-FFPE platform, we performed LC-MS/MS proteomics on CD20 targeted human tonsil slides. Pleasingly, CD20 and other known interactors were highly enriched (**Figure 4A**),⁴⁴ including SCR kinases, LYN and FYN, which are known to associate with B-cell surface receptors to enable signaling,⁴⁵ and many HLAs (DRA, DRB1/4).⁴⁶ Additionally, CD19, CD22, CD40 and CD79, known neighbors of CD20, were highly enriched.^{47,48} To understand any differences between FFPE tissue and a cellular model system, we performed μ Map-Blue with human PBMCs targeting CD20 (**Figure 4B**). Gratifyingly, CD20 and other top hits (CD40 and MHCs) were enriched in both the PBMCs and tonsil datasets. Despite this overlap, certain proteins that were highly enriched in tonsils were not observed in PBMCs, underscoring fundamental differences in B-cells between cells and human tissue. We then conducted an extensive comparison between tissue and cells, as well as healthy and diseased model systems. To this end, we

extended labeling to diseased B-cell lines (using μ Map-Blue) and diffuse large B-cell lymphoma (DLBCL) lymph nodes (using μ Map-FFPE). Interestingly, CD20 and other common neighbors were highly enriched across all data sets, supporting a common interactome. However, significant differences could be seen between model types. For example, CD38 and TRIM21 were uniquely enriched in cellular models, whereas CD22/79, ADAM10, LYN, and CD6 were only seen in tissues. Certain tissue-specific interactors can be explained by cell type heterogeneity, as CD6 is a common T-cell marker.⁴⁹ Furthermore, intracellular interactors, like LYN, can be identified in tissue because these samples have been permeabilized, enabling diffusion of the labeling intermediate into intracellular compartments. Finally, disease-specific proximal proteins were consistently identified in DLBCL tissue and cancer cell lines, illustrating the power of this technology to identify new neighboring proteins with potential pathological relevance (**Figure 4C**).

To validate these novel proximal proteins found in the tonsil CD20 microenvironment, we utilized STED microscopy. As a positive control, we examined the known interaction of CD20 and IgD, which showed colocalization in FFPE tonsil ($r = 0.669$).⁵⁰ Across triplicate μ Map-FFPE experiments targeting CD20 in tonsil, 10 proteins were consistently enriched including known interactors like many HLAs. Yet, this dataset also contained proteins that, to our knowledge, have not been identified within the CD20 microenvironment.^{47,48} These include ADAM10, CR1, CR2, and PTPCR. Using STED, we validated the colocalization of all these proteins with CD20 ($r = 0.524$ – 0.69), establishing μ Map-FFPE as tool for identifying novel protein microenvironments in preserved tissue samples (**Figure 5**). The CD20/ADAM10 interaction is of interest, as ADAM10 is a metalloprotease responsible for cleaving membrane-bound proteins, generating their soluble form. The loss of membrane bound CD20, driven by a range of mechanisms,⁵¹ is a well characterized resistance pathway for treatments targeting CD20.

Although further functional studies are required, understanding this interaction may suggest an orthogonal, ADAM10-mediated resistance pathway.

In conclusion, we have developed a photoproximity labeling technique, μ Map-FFPE, compatible with the vast libraries of preserved human tissue samples. Utilizing a red-light activated catalytic manifold and thermally stable probe was key to the realization of this technology. Furthermore, we illustrated key differences between biological model systems, highlighting the possibility of differential interaction networks between cells and tissues. Finally, new CD20 interactors were validated by STED. Ongoing efforts include probing changes to interaction networks before and after treatment for greater insight into mechanisms of drug resistance. Collectively, μ Map-FFPE serves as a new tool within the field of proximity labeling, situated to prosecute protein interactions in FFPE samples across biological contexts and disease states.

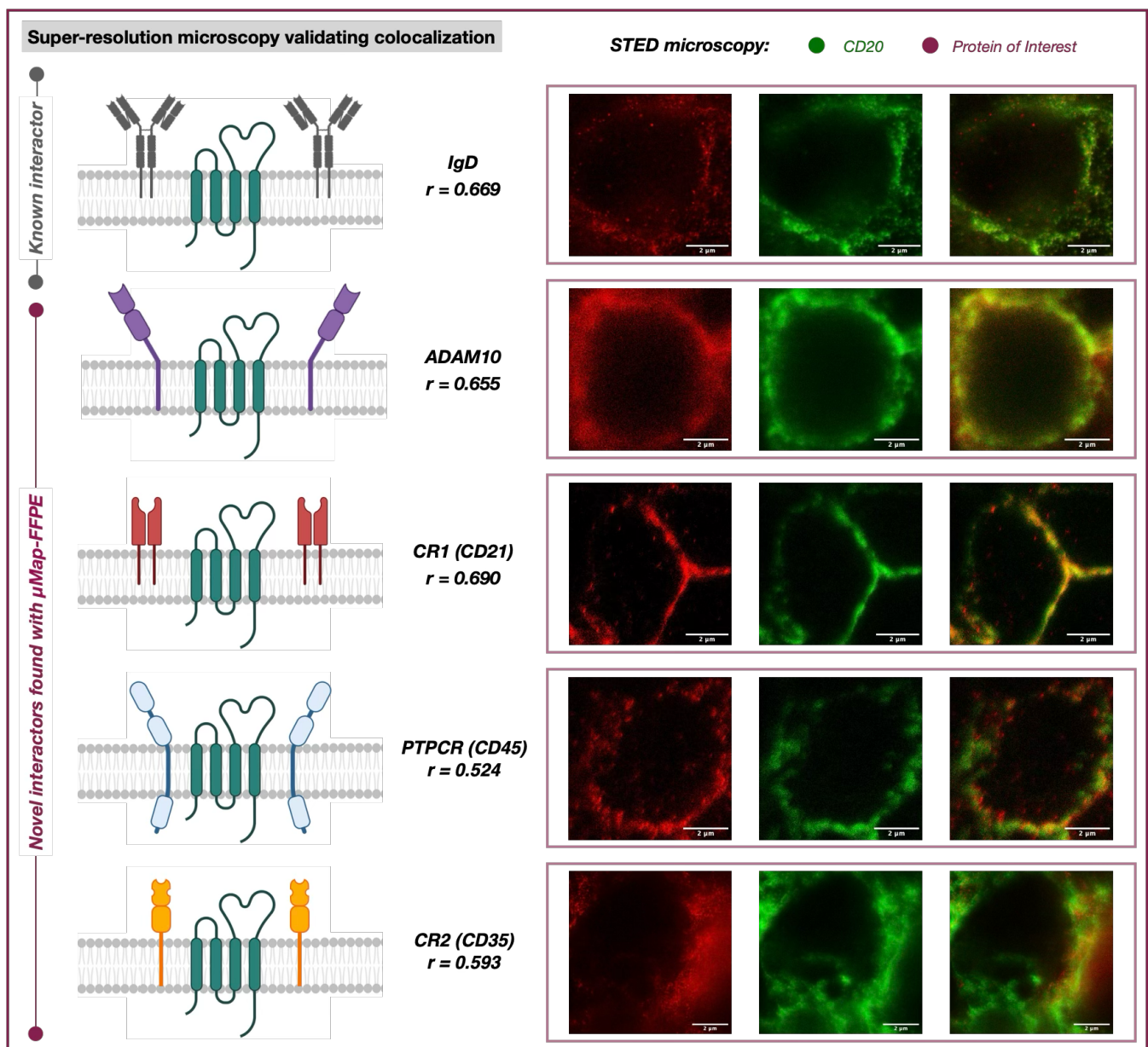


Figure 5: Validation of novel CD20 neighbors in FFPE tonsil using STED (r = Pearson's Coefficient).

ASSOCIATED CONTENT

Supporting Information

The Supporting Information is available free of charge on the ACS Publications website.

Supporting Information (PDF)

Combined Raw Proteomics Data – CD20 Labeling (XLSX)

Proteomics Data for BSA Labeling (XLSX)

AUTHOR INFORMATION

Corresponding Author

David W. C. MacMillan – Merck Center for Catalysis at Princeton University, Princeton, New Jersey 08544, United States
ORCID: <https://orcid.org/0000-0001-6447-0587>
Email: dmacmill@princeton.edu

Authors

Noah B. Bissonnette – Merck Center for Catalysis at Princeton University, Princeton, New Jersey 08544, United States
ORCID: <https://orcid.org/0000-0001-6892-5040>

Marie E. Zamanis – Genmab US, Inc., Building 2, 777 Scudders Mill Rd, Princeton, NJ 08540, United States

Steven D. Knutson – Merck Center for Catalysis at Princeton University, Princeton, New Jersey 08544, United States

Zane Boyer – Merck Center for Catalysis at Princeton University, Princeton, New Jersey 08544, United States
ORCID: <https://orcid.org/0009-0002-3739-9134>

Angelo Harris – Genmab US, Inc., Building 2, 777 Scudders Mill Rd, Princeton, NJ 08540, United States

Daniel Martin – Genmab US, Inc., Building 2, 777 Scudders Mill Rd, Princeton, NJ 08540, United States

Jacob B. Geri – Merck Center for Catalysis at Princeton University, Princeton, New Jersey 08544, United States
ORCID: <https://orcid.org/0000-0002-9215-5610>

Suzana Couto – Genmab US, Inc., Building 2, 777 Scudders Mill Rd, Princeton, NJ 08540, United States

Tahamtan Ahmadi – Genmab US, Inc., Building 2, 777 Scudders Mill Rd, Princeton, NJ 08540, United States

Anantharaman Muthuswamy – Genmab US, Inc., Building 2, 777 Scudders Mill Rd, Princeton, NJ 08540, United States

Mark Fereshteh – Genmab US, Inc., Building 2, 777 Scudders Mill Rd, Princeton, NJ 08540, United States

Notes

The authors declare the following competing financial interest(s): D.W.C.M. declares a competing financial interest with respect to the integrated photoreactor.

ACKNOWLEDGMENT

Research reported in this work was supported by the National Institute of General Medical Sciences of the National Institutes of Health (R35GM134897), the Princeton Catalysis Initiative, and kind gifts from Genmab. N.B.B. and Z.B. thank the Taylor family for the Edward C. Taylor Fellowship. The authors thank Brandon J. Bloomer and Sean W. Huth for helpful scientific discussions and Rebecca Lambert for assistance in preparing the manuscript.

ABBREVIATIONS

FFPE, formalin-fixed paraffin-embedded; Bt-Dz, biotin diazotane; Bt-Az, biotin azide; Bt-An, biotin aniline; BSA, bovine serum albumin; CA, carbonic anhydrase; DDA, data-dependent acquisition; DLBCL, diffuse large B-cell lymphoma; STED, stimulated emission depletion.

REFERENCES

- (1) De Las Rivas, J.; Fontanillo, C. Protein–Protein Interaction Networks: Unraveling the Wiring of Molecular Machines within the Cell. *Brief Funct Genomics* **2012**, *11*, 489–496.
- (2) Lu, H.; Zhou, Q.; He, J.; Jiang, Z.; Peng, C.; Tong, R.; Shi, J. Recent Advances in the Development of Protein–Protein Interactions Modulators: Mechanisms and Clinical Trials. *Signal Transduct. Target. Ther.* **2020**, *5*, 213.
- (3) Shin, W. H.; Kumazawa, K.; Imai, K.; Hirokawa, T.; Kihara, D. Current Challenges and Opportunities in Designing Protein–Protein Interaction Targeted Drugs. *Adv. Appl. Bionform. Chem.* **2020**, *13*, 11–25.
- (4) Greenblatt, J. F.; Alberts, B. M.; Krogan, N. J. Discovery and Significance of Protein–Protein Interactions in Health and Disease. *Cell* **2024**, *187*, 6501–6517.
- (5) Bledsoe, M. J.; Grizzle, W. E. The Use of Human Tissues for Research: What Investigators Need to Know. *Altern. Lab Anim.* **2022**, *50*, 265–274.
- (6) Junhee Seok; H. Shaw Warren; Alex, G. C.; Michael, N. M.; Henry, V. B.; Xu, W.; Richards, D. R.; McDonald-Smith, G. P.; Gao, H.; Hennessy, L.; Finnerty, C. C.; López, C. M.; Honari, S.; Moore, E. E.; Minei, J. P.; Cuschieri, J.; Bankey, P. E.; Johnson, J. L.; Sperry, J.; Nathens, A. B.; Billiar, T. R.; West, M. A.; Jeschke, M. G.; Klein, M. B.; Gamelli, R. L.; Gibran, N. S.; Brownstein, B. H.; Miller-Graziano, C.; Calvano, S. E.; Mason, P. H.; Cobb, J. P.; Rahme, L. G.; Lowry, S. F.; Maier, R. V.; Moldawer, L. L.; Herndon, D. N.; Davis, R. W.; Xiao, W.; Tompkins, R. G. Genomic Responses in Mouse Models Poorly Mimic Human Inflammatory Diseases. *Proc Natl Acad Sci U S A* **2013**, *110*, 3507–3512.
- (7) Vargas-Rondón, N.; Pérez-Mora, E.; Villegas, V. E.; Rondón-Lagos, M. Role of Chromosomal Instability and Clonal Heterogeneity in the Therapy Response of Breast Cancer Cell Lines. *Cancer Biol Med* **2020**, *17*, 970–985.
- (8) Altschuler, S. J.; Wu, L. F. Cellular Heterogeneity: When Do Differences Make a Difference? *Cell* **2010**, *141*, 559–563.
- (9) Sun, D.; Gao, W.; Hu, H.; Zhou, S. Why 90% of Clinical Drug Development Fails and How to Improve It? *Acta Pharm Sin B* **2022**, *12*, 3049–3062.
- (10) Akbarzadeh, S.; Coşkun, Ö.; Günçer, B. Studying Protein–Protein Interactions: Latest and Most Popular Approaches. *J Struct Biol* **2024**, *216*, 108118.

- (11) Geri, J. B.; Oakley, J. V.; Reyes-Robles, T.; Wang, T.; McCarver, S. J.; White, C. H.; Rodriguez-Rivera, F. P.; Parker Jr., D. L.; Hett, E. C.; Fadeyi, O. O.; Oslund, R. C. Microenvironment Mapping via Dexter Energy Transfer on Immune Cells. *Science (1979)* **2020**, *367*, 1091–1097.
- (12) Knutson, S. D.; Buksh, B. F.; Huth, S. W.; Morgan, D. C.; MacMillan, D. W. C. Current Advances in Photocatalytic Proximity Labeling. *Cell Chem Biol* **2024**, *31*, 1145–1161.
- (13) Fang, Y.; Zou, P. Photocatalytic Proximity Labeling for Profiling the Subcellular Organization of Biomolecules. *ChemBioChem* **2023**, *24*, e202200745.
- (14) Hananya, N.; Ye, X.; Koren, S.; Muir, T. W. A Genetically Encoded Photoproximity Labeling Approach for Mapping Protein Territories. *Proc Natl Acad Sci U S A* **2023**, *120*, e2219339120.
- (15) Zheng, F.; Zhou, X.; Zou, P.; Yu, C. Genetically Encoded Photocatalytic Protein Labeling Enables Spatially-Resolved Profiling of Intracellular Proteome. *Nat. Commun.* **2023**, *14*, 2978.
- (16) Pan, C.; Knutson, S. D.; Huth, S. W.; MacMillan, D. W. C. μ Map Proximity Labeling in Living Cells Reveals Stress Granule Disassembly Mechanisms. *Nat. Chem. Biol.* **2024**.
- (17) Knutson, S. D.; Pan, C. R.; Bisballe, N.; Bloomer, B. J.; Raftopolous, P.; Saridakis, I.; MacMillan, D. W. C. Parallel Proteomic and Transcriptomic Microenvironment Mapping (μ Map) of Nuclear Condensates in Living Cells. *J. Am. Chem. Soc.* **2024**, *147*, 488–497.
- (18) Buksh, B. F.; Knutson, S. D.; Oakley, J. V.; Bissonnette, N. B.; Oblinsky, D. G.; Schwoerer, M. P.; Seath, C. P.; Geri, J. B.; Rodriguez-Rivera, F. P.; Parker, D. L.; Scholes, G. D.; Ploss, A.; Macmillan, D. W. C. μ Map-Red: Proximity Labeling by Red Light Photocatalysis. *J. Am. Chem. Soc.* **2022**, *144*, 6154–6162.
- (19) Ryu, K. A.; Reyes-Robles, T.; Wyche, T. P.; Bechtel, T. J.; Bertoch, J. M.; Zhuang, J.; May, C.; Scandore, C.; Dephore, N.; Wilhelm, S.; Quasem, I.; Yau, A.; Ingale, S.; Szendrey, A.; Duich, M.; Oslund, R. C.; Fadeyi, O. O. Near-Infrared Photoredox Catalyzed Fluoroalkylation Strategy for Protein Labeling in Complex Tissue Environments. *ACS Catal* **2024**, *14*, 3482–3491.
- (20) Liu, Z.; Guo, F.; Zhu, Y.; Qin, S.; Hou, Y.; Guo, H.; Lin, F.; Chen, P. R.; Fan, X. Bioorthogonal Photocatalytic Proximity Labeling in Primary Living Samples. *Nat. Commun.* **2024**, *15*, 2712.
- (21) Lou, Z.; Zhang, Y.; Liang, X.; Cao, M.; Ma, Y.; Chen, P. R.; Fan, X. Deep-Red and Ultrafast Photocatalytic Proximity Labeling Empowered In Situ Dissection of Tumor-Immune Interactions in Primary Tissues. *J. Am. Chem. Soc.* **2025**, *147*, 9716–9726.
- (22) Tong, F.; Zhou, W.; Janiszewska, M.; Seath, C. P. Multi-probe Photoproximity Labeling of the EGFR Interactome in Glioblastoma Using Red-Light. *J. Am. Chem. Soc.* **2025**, *147*, 9316–9327.
- (23) Koh, J. M. S.; Sykes, E. K.; Rukhaya, J.; Anees, A.; Zhong, Q.; Jackson, C.; Panizza, B. J.; Reddel, R. R.; Balaine, R. L.; Hains, P. G.; Robinson, P. J. The Effect of Storage Time and Temperature on the Proteomic Analysis of FFPE Tissue Sections. *Clin Proteomics* **2025**, *22*, 5.
- (24) Sah, S.; Chen, L.; Houghton, J.; Kempainen, J.; Marko, A. C.; Zeigler, R.; Latham, G. J. Functional DNA Quantification Guides Accurate Next-Generation Sequencing Mutation Detection in Formalin-Fixed, Paraffin-Embedded Tumor Biopsies. *Genome Med* **2013**, *5*, 77.
- (25) Blow, N. Tissue Issues. *Nature* **2007**, *448*, 959–960.
- (26) Nirmalan, N. J.; Harnden, P.; Selby, P. J.; Banks, R. E. Mining the Archival Formalin-Fixed Paraffin-Embedded Tissue Proteome: Opportunities and Challenges. *Mol. Biophys.* **2008**, *4*, 712–720.
- (27) Casan, J. M. L.; Wong, J.; Northcott, M. J.; Opat, S. Anti-CD20 Monoclonal Antibodies: Reviewing a Revolution. *Hum. Vaccin. Immunother.* **2018**, *14*, 2820–2841.
- (28) Dabkowska, A.; Domka, K.; Firczuk, M. Advancements in Cancer Immunotherapies Targeting CD20: From Pioneering Monoclonal Antibodies to Chimeric Antigen Receptor-Modified T Cells. *Front. Immunol.* **2024**, *15*, 1363102.
- (29) Bückers, J.; Kastrup, L.; Wildanger, D.; Vicidomini, G.; Hell, S. W. Simultaneous Multi-Lifetime Multi-Color STED Imaging for Colocalization Analyses. *Opt. Express* **2011**, *19*, 3130–3143.
- (30) Magdeldin, S.; Yamamoto, T. Toward Deciphering Proteomes of Formalin-Fixed Paraffin-Embedded (FFPE) Tissues. *Proteomics* **2012**, *12*, 1045–1058.
- (31) García-Vence, M.; Chantada-Vazquez, M. del P.; Sosa-Fajardo, A.; Agra, R.; Barcia de la Iglesia, A.; Otero-Glez, A.; García-González, M.; Cameselle-Teijeiro, J. M.; Nuñez, C.; Bravo, J. J.; Bravo, S. B. Protein Extraction From FFPE Kidney Tissue Samples: A Review of the Literature and Characterization of Techniques. *Front. Med.* **2021**, *8*, 657313.
- (32) Kawashima, Y.; Kodera, Y.; Singh, A.; Matsumoto, M.; Matsumoto, H. Efficient Extraction of Proteins from Formalin-Fixed Paraffin-Embedded Tissues Requires Higher Concentration of Tris(Hydroxymethyl)Aminomethane. *Clin. Proteom.* **2014**, *11*, 4.
- (33) Boyer, J. H.; Canter, F. C. Alkyl and Aryl Azides. *Chem. Rev.* **1954**, *54*, 1–57.
- (34) Smolinsky, G. Thermal Reactions of Substituted Aryl Azides: The Nature of the Azene Intermediate. *J. Am. Chem. Soc.* **1961**, *83*, 2489–2493.
- (35) Tay, N. E. S.; Ryu, K. A.; Weber, J. L.; Olow, A. K.; Cabanero, D. C.; Reichman, D. R.; Oslund, R. C.; Fadeyi, O. O.; Rovis, T. Targeted Activation in Localized Protein Environments via Deep Red Photoredox Catalysis. *Nat. Chem.* **2022**, *15*, 101–109.
- (36) Zhang, Y.; Tan, J.; Chen, Y. Visible-Light-Induced Protein Labeling in Live Cells with Aryl Azides. *Chem. Commun.* **2023**, *59*, 2413–2420.
- (37) Victora, G. D.; Nussenzweig, M. C. Germinal Centers. *Annu. Rev. Immunol.* **2022**, *40*, 413–442.
- (38) Cook, K. M. Determining the Redox Potential of a Protein Disulphide Bond. In *Functional Disulphide Bonds*; Hogg, P., Ed.; Humana: New York, 2019; pp 65–86.
- (39) Nakane, K.; Sato, S.; Niwa, T.; Tsushima, M.; Tomoshige, S.; Taguchi, H.; Ishikawa, M.; Nakamura, H. Proximity Histidine Labeling by Umpolung Strategy Using Singlet Oxygen. *J. Am. Chem. Soc.* **2021**, *143*, 7726–7731.
- (40) Qiu, S.; Li, W.; Deng, T.; Bi, A.; Yang, Y.; Jiang, X.; Li, J. P. Ru(Bpy)₃²⁺-Enabled Cell-Surface Photocatalytic Proximity Labeling toward More Efficient Capture of Physically Interacting Cells. *Angew. Chem. Int. Ed.* **2023**, *62*, e202303014.
- (41) Miura, K.; Niimi, H.; Niwa, T.; Taguchi, H.; Nakamura, H. Intracellular Photocatalytic Proximity Labeling (IPPL) for Dynamic Analysis of Chromatin-Binding Proteins Targeting Histone H3. *ACS Chem. Biol.* **2024**, *19*, 2412–2417.
- (42) Nakane, K.; Nagasawa, H.; Fujimura, C.; Koyanagi, E.; Tomoshige, S.; Ishikawa, M.; Sato, S. Switching of Photocatalytic Tyrosine/Histidine Labeling and Application to Photocatalytic Proximity Labeling. *Int. J. Mol. Sci.* **2022**, *23*, 11622.

- (43) Matsukawa, R.; Yamane, M.; Kanai, M. Histidine Photooxygenation Chemistry: Mechanistic Evidence and Elucidation. *Chem. Rec.* **2023**, *23*, e202300198.
- (44) Pavlasova, G.; Mraz, M. The Regulation and Function of CD20: An “Enigma” of B-Cell Biology and Targeted Therapy. *Haematologica* **2020**, *105*, 1494–1506.
- (45) Deans, J. P.; Kalt, L.; Ledbetter, J. A.; Schieven, G. L.; Bolen, J. B.; Johnson, P. Association of 75/80-KDa Phosphoproteins and the Tyrosine Kinases Lyn, Fyn, and Lck with the B Cell Molecule CD20: Evidence against Involvement of the Cytoplasmic Regions of CD20. *J. Biol. Chem.* **1995**, *270*, 22632–22638.
- (46) Wilkinson, S. T.; Vanpatten, K. A.; Fernandez, D. R.; Brunhoeber, P.; Garsha, K. E.; Glinsmann-Gibson, B. J.; Grogan, T. M.; Teruya-Feldstein, J.; Rimsza, L. M. Partial Plasma Cell Differentiation as a Mechanism of Lost Major Histocompatibility Complex Class II Expression in Diffuse Large B-Cell Lymphoma. *Blood* **2012**, *119*, 1459–1467.
- (47) Szklarczyk, D.; Kirsch, R.; Koutrouli, M.; Nastou, K.; Mehryary, F.; Hachilif, R.; Gable, A. L.; Fang, T.; Doncheva, N. T.; Pyysalo, S.; Bork, P.; Jensen, L. J.; Von Mering, C. The STRING Database in 2023: Protein–Protein Association Networks and Functional Enrichment Analyses for Any Sequenced Genome of Interest. *Nucleic Acids Res.* **2023**, *51*, D638–D646.
- (48) Oughtred, R.; Rust, J.; Chang, C.; Breitkreutz, B. J.; Stark, C.; Willems, A.; Boucher, L.; Leung, G.; Kolas, N.; Zhang, F.; Dolma, S.; Coulombe-Huntington, J.; Chatr-aryamontri, A.; Dolinski, K.; Tyers, M. The BioGRID Database: A Comprehensive Biomedical Resource of Curated Protein, Genetic, and Chemical Interactions. *Protein Sci.* **2020**, *30*, 187–200.
- (49) Gonçalves, C. M.; Henriques, S. N.; Santos, R. F.; Carmo, A. M. CD6, a Rheostat-Type Signalosome That Tunes T Cell Activation. *Front. Immunol.* **2018**, *9*, 2994.
- (50) Kläsener, K.; Jellusova, J.; Andrieux, G.; Salzer, U.; Böhrler, C.; Steiner, S. N.; Albinus, J. B.; Cavallari, M.; Süß, B.; Voll, R. E.; Boerries, M.; Wollscheid, B.; Reth, M. CD20 as a Gatekeeper of the Resting State of Human B Cells. *Proc Natl Acad Sci U S A* **2021**, *118*, e2021342118.
- (51) Schuster, S. J.; Huw, L. Y.; Bolen, C. R.; Maximov, V.; Polson, A. G.; Hatzi, K.; Lasater, E. A.; Assouline, S. E.; Bartlett, N. L.; Budde, L. E.; Matasar, M. J.; Koeppen, H.; Piccione, E. C.; Wilson, D.; Wei, M. C.; Yin, S.; Penuel, E. Loss of CD20 Expression as a Mechanism of Resistance to Mosunetuzumab in Relapsed/Refractory B-Cell Lymphomas. *Blood* **2024**, *143*, 822–832.

Supplemental Figures

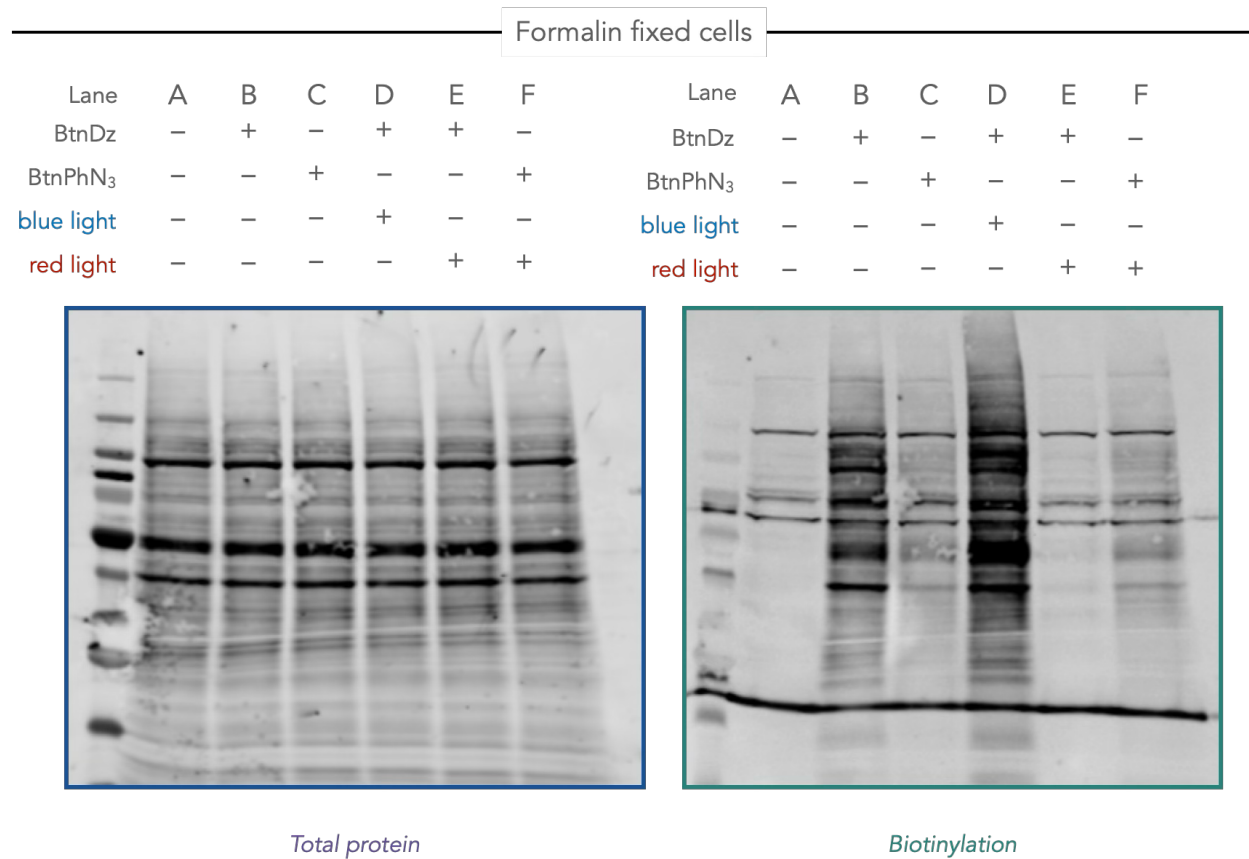


Figure S1: Background probe activation using cells fixed with formaldehyde in house.

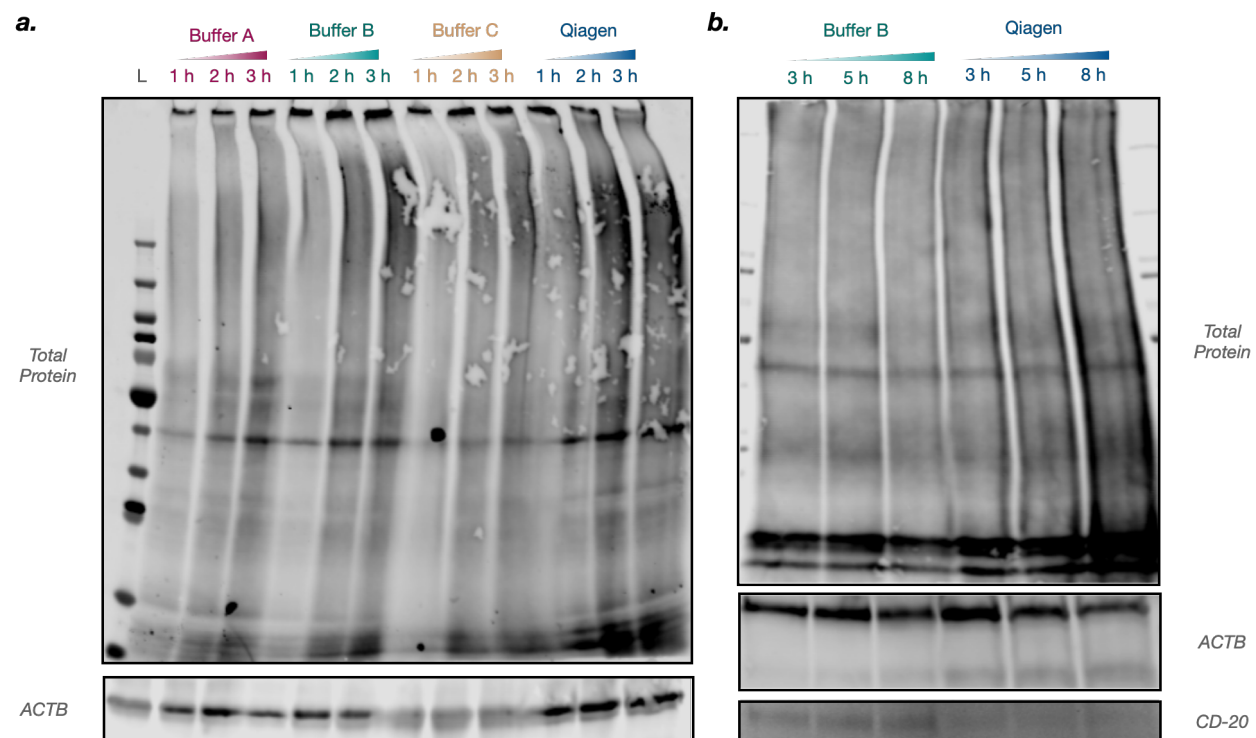


Figure S2: De-crosslinking optimization on tonsil tissue.

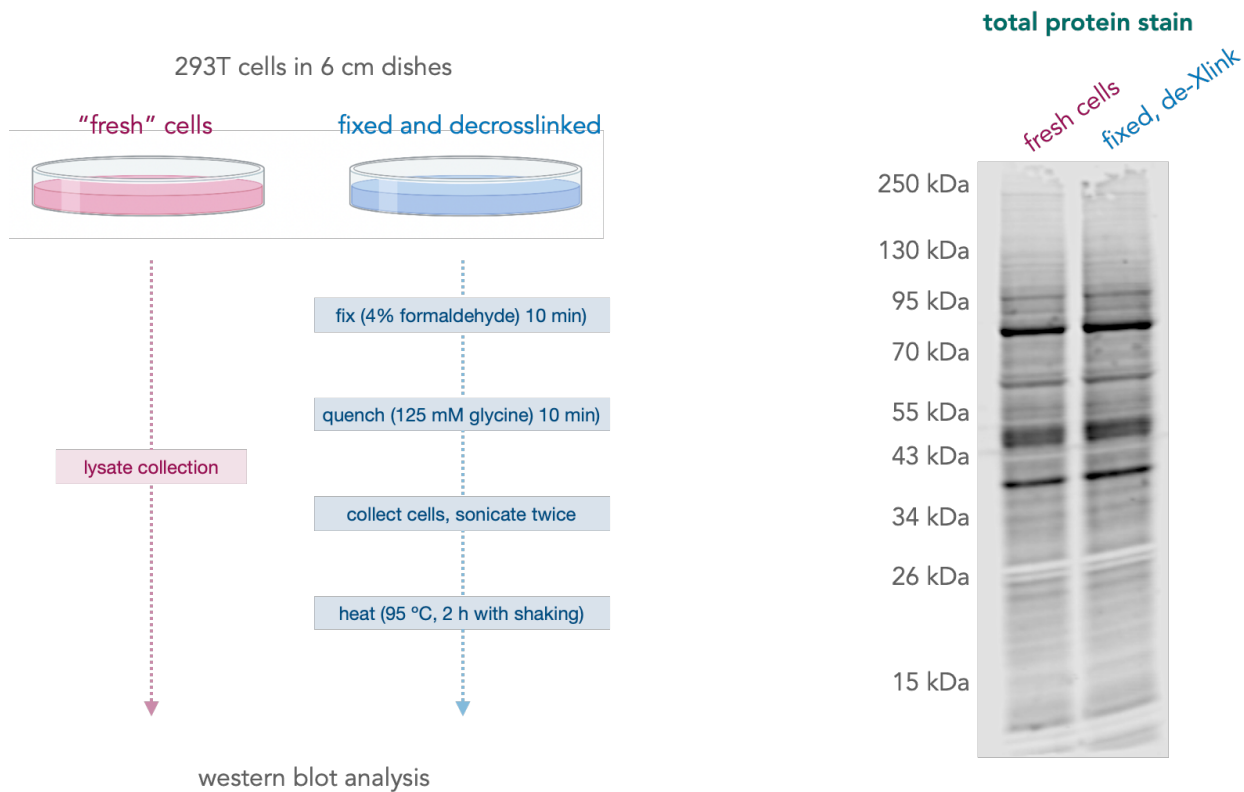


Figure S3: Crosslinking and de-crosslinking 293T cells.

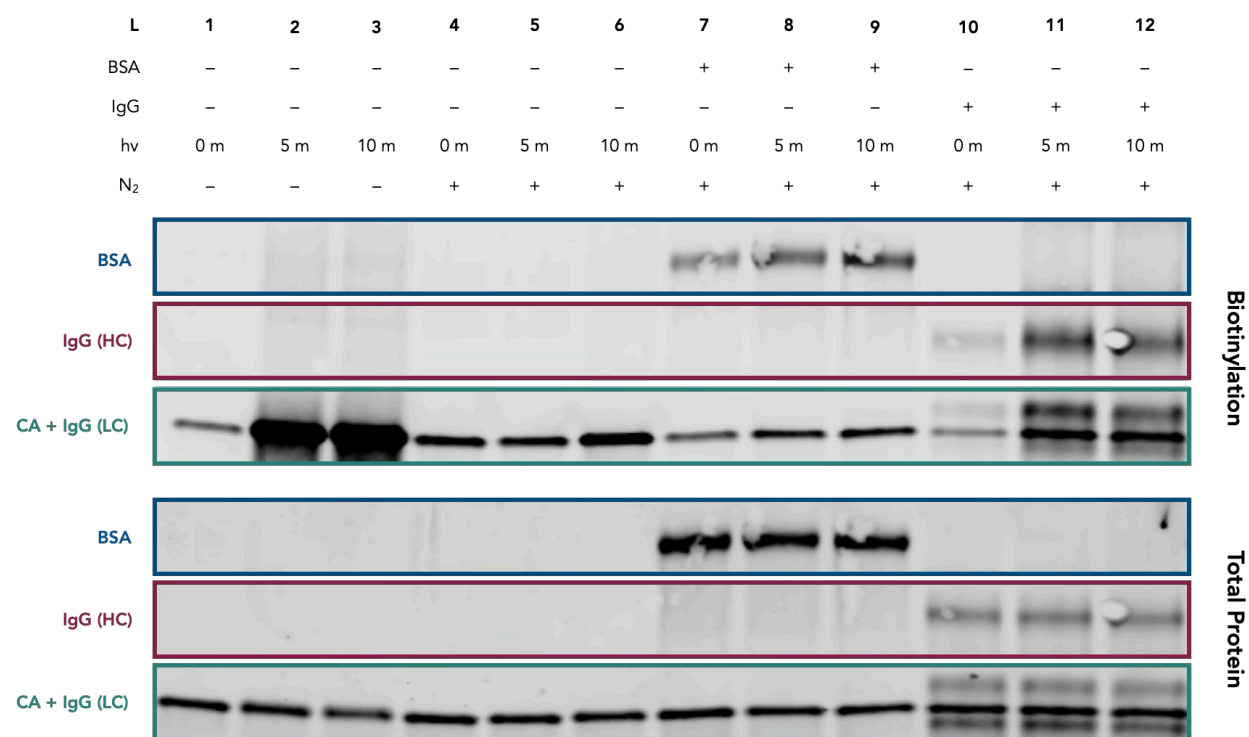


Figure S4: Disulfide containing biomolecules can turn on labeling under nitrogen.

Protocol for FFPE tissue labeling with label-free proteomic analysis

For proteomics runs, samples were run in triplicate. Slides were prepared with two tonsil sections per slide. 4 slides (8 total sections) were used per replicate for a total of 24 slides (triplicates for 1° and no 1° conditions).

Tissue Preparation: FFPE blocks were mounted on a Leica HistoCore Biocut Microtome and sectioned at a depth of 5 microns. The sectioned were placed in a Boekel Scientific Lighted Tissue Flotation Bath Model 145702 that was set to a temperature of 39.5°C. Two sections were mounted on SlideMate Laser Plus Slides and moved to a slide drying rack. The rack was placed (baked) in a Thermo Scientific HERATHERM Incubator at 60°C for 30 mins to melt some of the excess paraffin. The baked slides were then placed and agitated manually in a series of 2 xylene baths respectively for 30 seconds each. Finally, the slides were allowed to air dry in the fume hood for 30 mins.

Day 1 Labeling: Deparaffinized slides were heated to 55 °C for 30 min to remove residual water. Next slides were placed in a Coplin jar filled with Leica Bond Dewax and heated to 72 °C in an oven for 1 hr. Slides were then washed 3x with Leica reagent Alcohol by submersion in a 50 mL Falcon tube. Excess liquid was removed by tapping and the slides were briefly (~2 min) air dried. Next the slides were washed with Leica Bond 1X wash buffer 3x in the same manner. The perimeter of the slide was dried with a Kimwipe and a hydrophobic barrier was drawn with a pap pen. Next ~500 µL of Leica Enzymatic Epitope retrieval (1 drop per 7 mLs of Bond Enzyme Concentrate) was added to each slide and then incubated at 37 °C for 5 min. Slides were then placed in a Coplin jar containing MilliQ water and washed with Leica Bond 1X wash buffer 3x in 50 mL Falcon tubes. Afterwards, the slides were incubated in 500 µL of blocking buffer A (3% BSA, 0.05% Tween 20, 20 µg/mL Human Isotype IgG in DPBS) for 1 hr. The blocking solution was removed by aspirator and replaced with CD-20 mouse primary IgG (ab9475, 1:100 dilution in a 3% BSA, 0.05% Tween 20 in DPBS) for the directed slides and blocking buffer B (3% BSA, 0.05% Tween 20 in DPBS) for the control slides. The slides were incubated for 1 hr at room temperature. Next each slide was washed 3x with 500 µL Leica Bond 1X wash buffer. Each wash was incubated for 5 min and then removed from the slide *via* aspirator. Next 500 µL of SnChlorin-conjugated goat anti mouse secondary antibody (1 µg/mL in blocking buffer B) was added to each slide and incubated for 1 hr *in the dark* (Note: all steps until scraping tissue off the slides should be done in darkness, we typically place a box over the slides to protect them from ambient light). The secondary solution was removed by aspiration and the slides were washed with 500 µL of Leica Bond 1X wash buffer (4 x 5 min). In six distinct sets (each replicate), the final wash buffer was removed by aspiration, slides placed in the red light photoreactor and 500 µL of 1 mM biotin-aniline solution (in Leica Bond 1X wash buffer) was added. It is important to *ensure each slide is placed equidistant from the lights (2x2 grid)* to ensure even light distribution and intensity. Each set of slides was irradiated for 20 min then placed in a Coplin jar filled with MilliQ water in the dark. The slides were then washed with 500 µL of Leica Bond 1X wash buffer (3 X 5 min) and left in the dark overnight to dry.

Day 2 Extraction and Bead Pulldown: The hydrophobic barrier was removed by wiping with a methylene chloride-soaked paper towel or by scraping with a razor. Next the 24 slides (12 control, 12 directed) were scraped into six low bind Eppendorf tubes (4 slides per tube) and reconstituted in 600 µL of *freshly prepared* Lysis Buffer B (4% SDS w/v, 80 mM HEPES, 80 mM DTT, pH adjusted to 8 with aq NaOH). The tubes were then sonicated in the Bioruptor (high power, 30 sec on, 30 sec off, 10 cycles) after, they were next secured with a plastic clip and heated to 95 °C in a heating block with shaking for 1 hour. This sonication/heating cycle was repeated three more times (~4 hrs total). The tissue solutions were then hard pelleted at 4 °C (spinning at x15,000g for 15 min) and the supernatant was transferred to new Eppendorf tubes. These solutions may be stored at 4 °C for a few days if needed.

Protein concentration was next measured by dot blot vs BSA standards prepared in Lysis Buffer B to normalize sample concentration before pulldown. This step can be omitted if serial sections are utilized and all sections are approximately the same size. The same amount of total protein was added to 15 mL Falcon tubes and diluted 1:5 with 1X RIPA buffer. Next streptavidin coated magnetic beads (Pierce 88817) were equilibrated to room temperature and mixed well to ensure homogeneity. 300 µL of beads were transferred to a low bind Eppendorf tube then pelleted on a magnetic bead separation rack and the solution removed. The beads were then washed twice with 1 mL of equilibration buffer (1:5 Lysis Buffer B to RIPA 1X) by resuspending then pelleting on the magnetic rack and removing the supernatant. The beads were then resuspended in 300 µL equilibration buffer and 50 µL of bead solution was added to each 15 mL Falcon tube. The tubes were incubated overnight on a rotisserie at 4 °C.

Day 3 Bead Washing and Digest: The beads were next consolidated back to six, 1.5 mL low bind Eppendorf tubes by adding bead solution and removing supernatant. Following consolidation, the beads were washed (*via* resuspension, magnetic pelleting and supernatant removal) 3X with 1 mL 1% SDS in DPBS, 2X with 1 mL 1M NaCl in DPBS, 1X with 1 mL 10% EtOH in DBPS, and 3X with 1 mL 100 mM NH₄HCO₃ in MilliQ water. Next the beads were resuspended in 500 µL of 6 M urea in DBPS and 25 µL of 200 mM DTT in 25 mM NH₄HCO₃ and incubated at 37 °C on a rotisserie for 30 minutes. Subsequently, 30 µL of 500 mM IAA in 25 mM NH₄HCO₃ was added and the samples were incubated at room temperature *in the dark* on a rotisserie for 30 minutes. The beads were next pelleted on a magnetic rack and the supernatant was removed. The beads were next washed (*via* resuspension, magnetic pelleting and supernatant removal) 3X with 500 µL DBPS and 3X 500 µL 50 mM NH₄HCO₃. Afterwards the beads were resuspended in 500 µL 50 mM NH₄HCO₃ and transferred to six new low bind Eppendorf tubes. The beads were pelleted by magnetic separation and the supernatant removed. Finally, the beads were resuspended in 40 µL 50 mM NH₄HCO₃ and 2 µL of MS grade trypsin (1 mg/mL in 50 mM optima grade acetic acid) was added. The beads were then incubated overnight on a rotisserie at 37 °C).

Day 4 Proteomics: The beads were pelleted, and the *supernatant* (~40 µL) was transferred to six new low bind Eppendorf tubes. Each tube was acidified with 1 µL of optima grade formic acid and spin filtered into a new Eppendorf via centrifuging at x10,000 g for 5 min. These samples can be stored at -80 °C. Label-free, data independent analysis (DIA) proteomics was performed on a Bruker TIMS-TOF Pro 2 inline with a nanoElute LC. Per sample, 1 µL of enriched lysate was injected onto a trap column (C18 Pepmap, 5 µM particle size, 5 mm length, 300 µM internal diameter), followed by separation on an analytical column (C18 ReproSil AQ, 1.9µM particle size, 100 mm length, 75µM internal diameter). Peptides were eluted via a gradient consisting of MeCN/water at a column temperature of 40°C (buffer A = 0.1% formic acid/water, buffer B = 0.1% formic acid/MeCN; flow rate 0.5 µL/min; gradient; start at 2% B, then increase to 35% B over 20 min, increase to 95% B over 30 seconds, hold at 95% for 2.25 min.) Scans were performed in positive ion, dia-PASEF mode over a m/z range of 100-1700 with a ramp time of 100 ms, Accu. time of 100 ms, and a duty cycle of 100%, ramp rate of 9.43 Hz, MS averaging set to 1. Absolute thresholds were set to 5000 for mobility peaks and 10 for MS peaks.

The resulting raw data (.d files) were then processed via DIANN 18.8.112,13 via the following parameters: trypsin/P digestion, 3 missed cleavages, 3 max. variable modifications, N-term M excision, Ox(M), Ac(N-term) and C-carbamidomethylation, peptide length range of 7-30, precursor charge range 1-4, m/z range 300-1800, fragment ion range 200-1800, Mass accuracy and MS accuracy both set to 10, precursor FDR set to 1%. Within the DIANN algorithm, the following settings are applied: “Use isotopologues”, “MBR” (match between runs), “No shared spectra”, “Heuristic protein inference”. A spectra library was utilized which was generated from DIANN via all known human proteins (In-Silico spectral library – generated in DIANN via FASTA of Uniprot human proteome UP000005640 – options selected were “FASTA digest for library-free search/library generation” and “Deep learning-based spectra, RTs and IMs prediction’, other parameters same as describe above). After processing, resulting matrix.pg files were worked up in Perseus (v. 2.0.7.0). Intensities are inputted as “main” while the other descriptors are listed as “categorical”. Intensities were transformed by log base 2, and data was annotated to the appropriate condition (e.g. pre, active, post phagocytosis). At this point, normalization was performed via median subtraction, and a volcano plot was generated utilizing a t-test for statistical significance. Resulting volcano plots were plotted in GraphPad Prism 9 for final figures.